Specific Oxidative Dehydrogenation Reaction Mechanism over Vanadium(IV/III) Sites in TiO$_2$ with Uniform Mesopores under Visible Light[1]

Yasuo Izumi,[*1] **Kazushi Konishi,**[1,2] **and Hideaki Yoshitake**[3]

[1]Department of Chemistry, Graduate School of Science, Chiba University,
1-33 Yayoi, Inage-ku, Chiba 263-8522

[2]Interdisciplinary Graduate School of Science and Engineering, Tokyo Institute of Technology,
4259 Nagatsuta, Midori-ku, Yokohama 226-8502

[3]Graduate School of Engineering, Yokohama National University,
79-5 Tokiwadai, Hodogaya-ku, Yokohama 240-8501

Received March 10, 2008; E-mail: yizumi@faculty.chiba-u.jp

Selective oxidation under visible light is attractive for application in environment-benign societies. Oxidative dehydrogenation of ethanol proceeds over mesoporous V-doped TiO$_2$ under visible light in clear contrast to ethanol dehydrogenation over crystalline TiO$_2$ doped or undoped with V and inactive mesoporous TiO$_2$. The red-ox states of V^{IV} and V^{III} were detected using X-ray spectroscopies. In this paper, kinetic measurements of each catalytic step and X-ray spectroscopic monitoring under catalytic reaction conditions are correlated. The ethanol conversion to acetaldehyde in the absence of O$_2$ was monitored under visible light coupled with reduction of V^{IV} to V^{III} species based on V K$\beta_{5,2}$ emission and V K$\beta_{5,2}$-selecting X-ray absorption fine structure spectra. The oxidative dehydrogenation of dissociatively adsorbed ethoxyl species proceeded in O$_2$ under visible light with formation rates 38% of steady photo-catalysis in ethanol + O$_2$. The acetaldehyde desorption step by H subtraction from ethoxyl species on V^{III} was found to be rate-limiting. The origin of oxidative dehydrogenation over mesoporous V–TiO$_2$ was suggested to be coordinatively unsaturated V^{III} species specifically activating O$_2$ molecules. Further, a poisoning effect of product water was demonstrated to block the active V sites. UV light illumination was found to be effective to re-activate the mesoporous V–TiO$_2$ catalyst.

Semiconductors are used for the oxidative decomposition of volatile organic compounds (VOC) to protect/improve the atmospheric environment and for decomposition of dyes and industrial organic compounds to purify water environments.[2,3] Titanium dioxide is a representative semiconductor photo-catalyst.[4] To reduce the band gap (3.2 and 3.0 eV for anatase- and rutile-type TiO$_2$ crystallines, respectively) to the energy region of visible light and thus enable catalysis activated under visible light, new preparation routes and morphologies of TiO$_2$ have been intensively reported.[5] Various hetero atoms, e.g. C,[5] N,[6–8] F,[9] Al,[10] P, S,[11] V,[12,13] Cr,[12] Mn,[12] Fe,[12,14] Ni,[12] and I,[15,16] have been doped to anatase- and/or rutile-type TiO$_2$ crystallines to create impurity levels between the band gap. Mesoporous frameworks of TiO$_2$, both unadulterated and those doped with N,[7] F,[9] or V[13] have been less extensively tested for photo-catalysis. Mesoporous TiO$_2$ prepared both with and without organic templates[4,17] generally consists of smaller particles than those for crystallines, e.g. Degussa P25 (particle size 15–40 nm) and is affected by quantum size effects to widen the band gap.[12,13]

Oxidative detoxification of VOC is practical if it proceeds under activation by visible light. In this paper, ethanol was chosen as a representative VOC and tested for excitation under visible light. Selective, oxidative dehydrogenation of ethanol

was reported over mesoporous V–TiO$_2$ of narrow pore size distribution centered at 3 nm.[13] The specific surface area (SA) was 1000 m^2 g^{-1} and it catalytically produced acetaldehyde and water. Mesoporous TiO$_2$ with a specific SA of 1200 m^2 g^{-1} was found to be essentially inactive. The dehydrogenation reaction proceeded to form acetaldehyde only over V-doped or undoped crystalline TiO$_2$ (P-25) under visible light. The mesoporous V–TiO$_2$ is advantageous for X-ray spectroscopic study because the V^{IV} sites substitute on the Ti sites of TiO$_2$ matrix and distribute homogeneously. When the V/Ti atomic ratio was 1/21, only V^{IV} species coordinated to 4–5 oxygen atoms was detected.[18] The V-doped mesoporous TiO$_2$ is expected to perform selective O$_2$ molecule activation.

V K$\beta_{5,2}$-selecting V K-edge X-ray absorption fine structure (XAFS) detected V^{IV} and V^{III} states independently under catalytic reaction conditions.[19] The V K$\beta_{5,2}$ fluorescence emitted from the catalysts was analyzed using high energy-resolution fluorescence spectrometry and structural and electronic information of the V sites were given state-selectively. On-reaction monitoring of valence and structure changes for active V sites had not been performed yet.

In this paper, kinetic measurements for each reaction step and on-reaction X-ray spectroscopic monitoring were correlated to clarify the reaction mechanism of ethanol oxidative
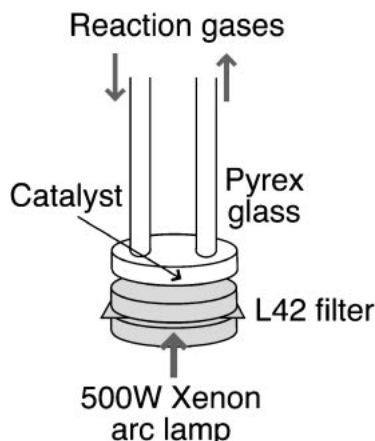
Scheme 1. Photo-catalytic reaction cell and visible light illumination.

dehydrogenation over mesoporous V–TiO$_2$ under visible light. The V states were monitored by on-reaction V K$\beta_{5,2}$ emission and V K$\beta_{5,2}$-selecting V K-edge XAFS spectroscopies. In addition, the poisoning effect of product water was kinetically confirmed and structurally monitored by the V^{III}/V^{IV}-state selective XAFS spectroscopy. Then, repeated catalysis tests were performed over mesoporous V–TiO$_2$ by illuminating UV–visible light between reaction batches.

Experimental

Sample Preparation.   Vanadium metal (25 μm thickness, 99.7%; Aldrich) and V$_2$O$_3$ (99.99%, Aldrich) were used as received. The V$_2$O$_3$ powder was thoroughly mixed with boron nitride (Wako) under argon to 3.0 wt % of V and pressed into a 20 mm-diameter disk.

The preparation route of mesoporous V–TiO$_2$ catalysts was followed from literature.[20] In brief, water was added dropwise to a mixture of vanadium triisopropoxide oxide, titanium tetraisopropoxide, and dodecylamine at 273 K. 0.1 M HCl was added. The suspension was maintained at 333 K for 4 days. Then, the solution was filtered and washed with methanol and diethyl ether. The obtained powder was heated under vacuum at 453 K for 2 h and sealed. The sample was kept at 453 K for 10 days and then washed with *p*-toluenesulfonic acid in ethanol. The V content was fixed to 3.0 wt %, corresponding to a V/Ti atomic ratio of 1/21.

Kinetic Tests.   A hundred milligrams of catalyst was evacuated in a branched, flat pillbox shaped quartz reaction cell (bottom area 23.8 cm^2; Scheme 1) at 10^{-6} Pa for 2 h at 290 K. Ethanol oxidation was performed in a closed circulating system (internal volume 100 mL) connected to the reaction cell and illuminated using a xenon short arc lamp operated at 400 W (UXL-500D, Ushio; Scheme 1). A UV-cut filter L42 (>420 nm; Kenko) was set at the light exit, 2 mm from the bottom of quartz reaction cell. UV-cut filters (Kenko) L-37 (>370 nm), Y-48 (>480 nm), Y-52 (>520 nm), and O-58 (>580 nm) were also used to observe the catalytic reactivity dependence on wavenumber. The products and reactants were analyzed using an online gas chromatograph equipped with a thermal conductivity detector (Shimadzu GC-8AT) and Porapak-Q column (GL Sciences). The change of oxygen gas pressure was monitored using a capacitance manometer (CCMT-1000A, ULVAC).

1.33 kPa of ethanol and 2.67 kPa of oxygen were introduced to the reaction system. Control photo-catalytic kinetic measurements were performed under 1.33 kPa of ethanol over fresh mesoporous V–TiO$_2$ or under 1.33 or 2.67 kPa of oxygen over mesoporous V–TiO$_2$, ethanol-pre-adsorbed. The pre-adsorption was performed under 1.50 kPa of ethanol for 15 min followed by evacuated at 10^{-6} Pa for 15 min at 290 K. Separately, 1.73 kPa of water was introduced to the catalyst for 15 min, evacuated at 10^{-6} Pa for 15 min, and then 1.33 kPa of ethanol and 2.67 kPa of O$_2$ were introduced for kinetic tests all at 290 K.

Reactivation of ethanol oxidation catalyst was tested by repeating reaction batches for 5 h. Between each reaction batch, mesoporous V–TiO$_2$ was evacuated at 10^{-6} Pa under the illumination of a xenon short arc lamp without a UV-cut filter.

X-ray Measurements.   The X-ray measurements were performed in the Photon Factory at the High-Energy Accelerator Research Organization (Tsukuba) on a bending-magnet beamline 7C at 290 K. The storage-ring energy was 2.5 GeV and the ring current was between 449 and 238 mA. A Si(111) double crystal monochromator and a higher-harmonics-rejection mirror of fused silica were inserted into the X-ray beam path. The X-ray beam was focused at the sample position, 490 mm from the X-ray beam exit of the vacuum beam duct, using the Sagittal-focusing mechanism and fully tuned using a Piezo translator.

The X-ray fluorescence emitted from samples was analyzed with a homemade fluorescence spectrometer.[18,19,21,22] A slit **0** was set in front of an ion chamber (S1194-B1, Oken) for the I_0 signal count. The ion chamber was purged with a mixture of helium and nitrogen (7:3). The sample was set on a plane tilted from the horizontal plane toward the incident X-ray beam by 6.0° and toward a spherically bent Johann-type Ge(422) analyzer crystal (Saint Gobain) by 7.0°. A slit **1** was set at 100 mm from the sample, between the sample and the Ge analyzer crystal. A slit **2** was set in front of the NaI(Tl) scintillation counter (SP10, Oken) for the I_f signal count. The slit opening size was 1.0×1.0 mm^2 for slit **0** and 8.0×8.0 mm^2 for slit **1** and slit **2**. The sample, slit **2**, and Ge analyzer crystal were vertically set in the Rowland configuration. The crystal's curvature radius was 450 mm. The spectrometer was purged with helium. The scintillation counter was purged with nitrogen gas to avoid discharging of the preamplifier. The sample section was covered with a 1 mm-thick lead plate housing, except for the openings for the incident X-ray beam and the exit of X-ray fluorescence from the sample to suppress the background of the I_f signal.

A hundred milligrams of mesoporous V–TiO$_2$ powder were pressed into a 20 mm-diameter disk. Each sample disk was set in an on-reaction cell equipped with 16 μm-thick polyethylene naphthalate windows (Q51-16, Teijin) and evacuated at 10^{-6} Pa for 3 h. Then, 77 kPa of argon or 0.37 kPa of water was introduced. Separately, the catalyst was in 4.3 kPa (constant) of ethanol by making a loop between the on-reaction cell and liquid ethanol storage (0.5 mL). The gas in the loop was mechanically circulated at a rate of 1 mL$_{gas}$ min^{-1}. The catalyst in constant flow of ethanol gas was illuminated 10 mm from the exit window of a Xe short arc lamp equipped with a L42 filter.

The V K$\beta_{5,2}$ emission spectra (X-ray fluorescence, XRF) were measured for V metal and mesoporous V–TiO$_2$ by scanning the fluorescence spectrometer with the excitation energy fixed at 5483.6 eV. The emission energy for the V metal was calibrated to 5462.9 eV (Bragg angle $\theta_B = 79.335°$).[23,24] The scan step of the emission energy was ≈0.36 eV and the accumulation time was 60–90 s per point. The count rates of emitted photons measured by scintillation counting were 10^2–10^1 and 10^1–10^0 counts s^{-1} for V metal and mesoporous V–TiO$_2$, respectively.
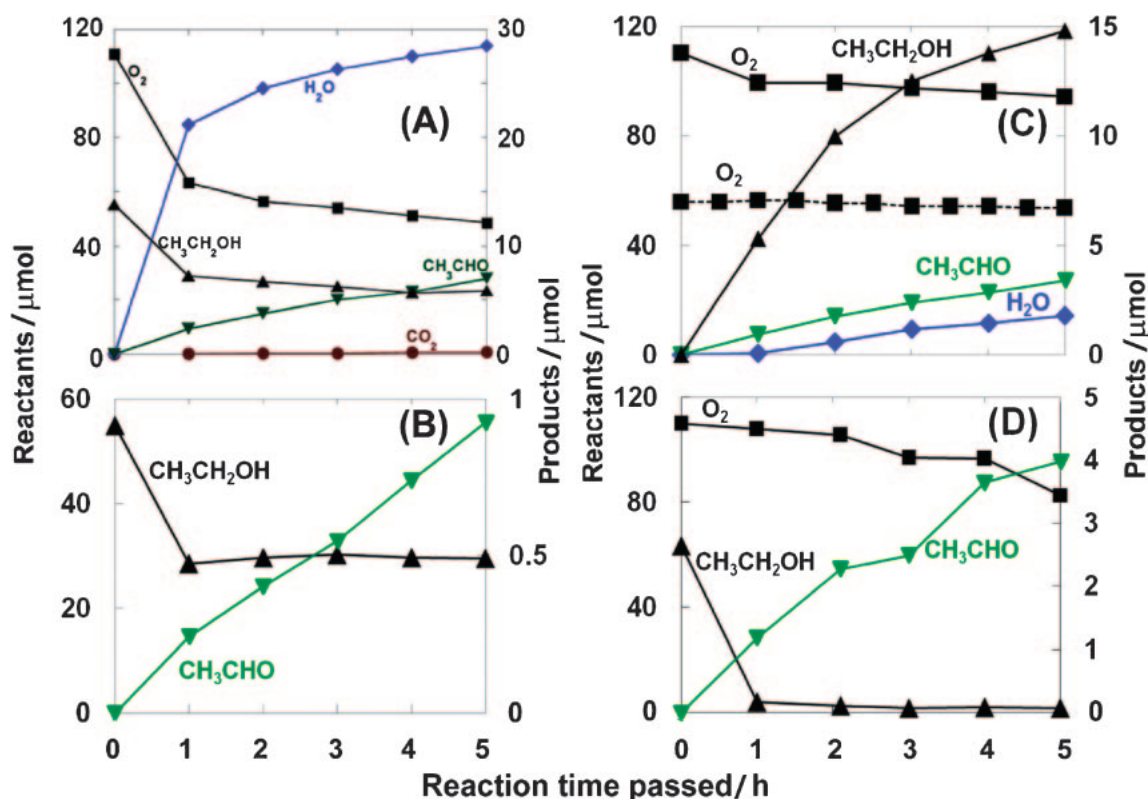
Figure 1. Time course of ethanol oxidation/decomposition reactions over mesoporous V–TiO$_2$ (3.0 wt % V). Visible light (>420 nm) was illuminated at 290 K. Initial concentrations were ethanol (1.33 kPa) + O$_2$ (2.67 kPa) (A and D), ethanol (1.33 kPa) (B), and O$_2$ (2.67 kPa) (C) in a closed circulating system (100 mL). Fresh catalyst (A and B) and catalyst in ethanol (1.50 kPa) (C) or water (1.73 kPa) (D) for 15 min and in vacuum for 15 min (C and D) were used (100 mg). The O$_2$ pressure change was monitored starting from initial 1.33 (dotted line) or 2.67 kPa of O$_2$ (solid line) and a liquid nitrogen trap was inserted in the reaction loop during catalytic test (C).

The V K$\beta_{5,2}$-selecting V K-edge XAFS spectrum was measured by tuning the fluorescence spectrometer to fixed emission energies around the V K$\beta_{5,2}$ emission peak. The scan step of photon energy was ≈0.25 eV and the accumulation time was 60–200 s per point. The V K-edge energy for V metal was calibrated to 5463.9 eV.[23,24] The energy positions of the monochromator and the fluorescence spectrometer were reproduced within the errors of ±0.1 and ±0.2 eV, respectively. Energy resolution of the fluorescence spectrometer was evaluated to be 1.1 eV at 5.5 keV.

Analysis. The XAFS data was analyzed with the software package XDAP version 2.2.7 (XAFS Services International) based on the works of M. Vaarkamp, H. Linders, and D. Koningsberger. The pre-edge background was approximated by the modified Victoreen function $C_2/E^2 + C_1/E + C_0$. The background of post-edge oscillations was approximated by a smoothing-spline function, calculated by the equation for the number of data points N.

$$\sum_{i=1}^{N} \frac{(\mu x_i - BG_i)^2}{\exp(-0.075k_i^2)} \leq \text{smoothing factor} \quad (1)$$

The similarity of XANES spectra (spectral fit) was evaluated based on the R-factor.

$$R_f = \int |\chi^{\text{observed data}}(k) - \chi^{\text{reference data}}(k)|^2 dk$$
$$\Big/ \int |\chi^{\text{observed data}}(k)|^2 dk \quad (2)$$

Results

Photo-Kinetics over Mesoporous V–TiO$_2$. The time course of photo-oxidation of ethanol over mesoporous V–TiO$_2$ catalyst under visible light (>420 nm) is shown in Figure 1A. The oxidative dehydrogenation proceeded over mesoporous V–TiO$_2$ to produce acetaldehyde and water. Initially water formation was quicker however after one hour acetaldehyde and water formation reached a steady state (Table 1, Entry A). The molar quantity of water formed in the first 1 h corresponded to 36% of the molar amount of V in the mesoporous V–TiO$_2$. Because the sample was evacuated for 2 h before the photo-catalysis and water formation in Figure 1A was repeated when the photo-catalysis batches were repeated, the water formation (initial, steady) was catalytic.

Comparable photo-catalytic tests in ethanol were performed in the absence of O$_2$ under visible light. Ethanol dehydrogenation proceeded to form acetaldehyde as a single product (Figure 1B). The formation rate was 10% of the oxidative dehydrogenation rate in ethanol + O$_2$ (Table 1, Entries A and B). This control reaction may consist of the first two steps of oxidative hydrogenation: dissociative adsorption of ethanol and H atom subtraction from the adsorbed ethoxyl species to evolve acetaldehyde.

Another control reaction was performed in oxygen (initial pressure 2.67 kPa) over ethanol pre-adsorbed mesoporous

Table 1.   Product Formation and Decomposition Rates in the Ethanol Photo-oxidation/Photo-decomposition over Mesoporous V–TiO$_2$ Catalyst[a] under Visible Light (>420 nm)

Entry	Catalyst	Reaction gas	Decomposition rates/μmol h^{-1} g$_{cat}$$^{-1}$ [b]	Formation rates/μmol h^{-1} g$_{cat}$$^{-1}$ [c]		
			O$_2$	CH$_3$CHO	H$_2$O	CO$_2$
A	Fresh	Ethanol (1.33 kPa) + O$_2$ (2.67 kPa)	—	23	212 (16)[d]	0.3
B		Ethanol (1.33 kPa)	—	2.4	0	0
C	Ethanol adsorbed[e]	O$_2$ (2.67 kPa)	15	8.8	6.1	0
C′		O$_2$ (1.33 kPa)	13	7.4	4.1	0
D	Water adsorbed[f]	Ethanol (1.33 kPa) + O$_2$ (2.67 kPa)	—	12	0	0

a) 3.0 wt % of V. b) Monitored using capacitance manometer. c) Monitored using gas chromatograph. d) Steady-state rate after 1 h of reaction. e) 1.50 kPa of ethanol was introduced for 15 min and catalyst placed under reduced pressure of 10^{-6} Pa for 15 min. f) 1.73 kPa of water was introduced for 15 min and catalyst placed under reduced pressure of 10^{-6} Pa for 15 min.
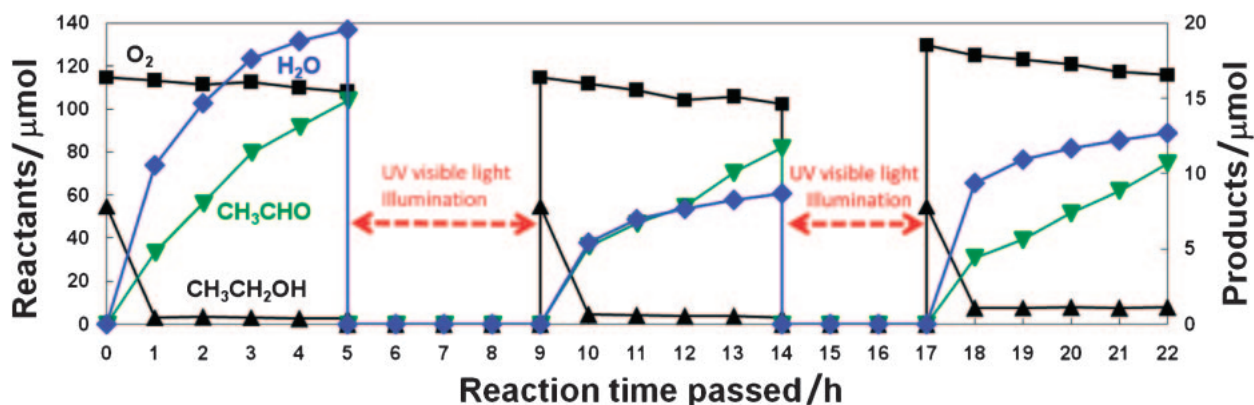
Figure 2.   Repeated reaction tests of ethanol oxidation under visible light over mesoporous V–TiO$_2$ (3.0 wt % V). The reaction conditions were similar to those for Figure 1A. A liquid nitrogen trap was inserted in the reaction loop during catalysis. After each reaction batch, the gas phase was evacuated and the catalyst was illuminated with UV–visible light from a xenon arc lamp operated at 400 W.

V–TiO$_2$ (Figure 1C). The steady formation rates of acetaldehyde and water were both 38% of the corresponding rates over fresh catalyst in ethanol + O$_2$ (Table 1, Entries A and C). The rate of reverse reaction to form reactant ethanol was faster: 51 μmol h^{-1} g$_{catalyst}$$^{-1}$. The O$_2$ decomposition rates did not correspond to formation rates of acetaldehyde and water because reverse reaction from ethoxyl adsorbed to ethanol proceeded and O$_2$ molecules may be consumed in other reaction(s).

The reaction for ethanol pre-adsorbed mesoporous V–TiO$_2$ was also performed in 1.33 kPa of O$_2$ (initial pressure). The consumption of oxygen is plotted in Figure 1C (dotted line) and consumption/formation rates are summarized in Table 1, Entry C′. The rates were 67–84% of the corresponding rates starting from 2.67 kPa of O$_2$ (Table 1, Entry C). Therefore, this reaction rate dependence on the O$_2$ pressure was less than one. The oxidation of ethoxyl species consists of more than two steps. The first step is H atom subtraction from the adsorbed ethoxyl species to evolve acetaldehyde and the next steps are the reaction of gaseous O$_2$ with remaining H atoms over the catalyst and the dissociation of O–O bonds.

Next, photo-oxidation tests were performed in ethanol (1.33 kPa) + O$_2$ (2.67 kPa) over water pre-adsorbed mesoporous V–TiO$_2$ (Figure 1D). The rate of O$_2$ consumption was slower than that observed with fresh catalyst (panel A). The

product was acetaldehyde only and the formation rate was 52% of the steady formation rate over untreated mesoporous V–TiO$_2$ (Table 1, Entries A and D). Thus, effective V sites for the O$_2$ adsorption/activation were partially blocked with water molecules.

Finally, photo-catalytic batch reactions were repeated (Figure 2). Between each batch, mesoporous V–TiO$_2$ catalyst was placed under vacuum (10^{-6} Pa) under UV–visible light. In the time course profile for the second and third batches, water was produced quicker in the first 1 h and then the formation rates of acetaldehyde and water reached a steady state, similar to the profile for the first batch. The formation rates of acetaldehyde and water (initial, steady) were 108, 52, and 23%, respectively, in the second batch and 93, 90, and 31%, respectively, in the third batch compared to corresponding rates in the first batch.

V K$\beta_{5,2}$ Emission Spectra.   The V K$\beta_{5,2}$ emission spectra were measured for mesoporous V–TiO$_2$ (Figure 3). A major peak for the fresh sample at 5462.1 eV (spectrum-a) shifted by −0.8 eV in 0.37 kPa of water (spectrum-b). A similar peak shift to lower energy (−0.5 eV) was reported for mesoporous V–TiO$_2$ in 2.1 kPa of ethanol (Table 2A).[19]

For the mesoporous V–TiO$_2$ in 4.3 kPa of ethanol (constant) under visible light, the time course change of V K$\beta_{5,2}$ emission spectra was monitored (Figures 3c–3f). Compared to the major
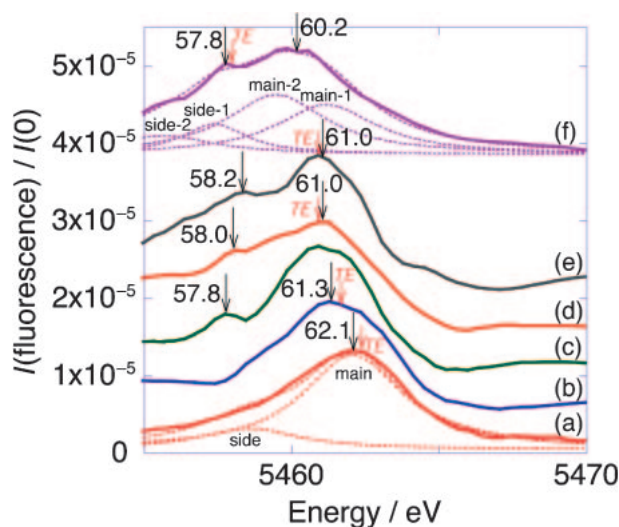
Figure 3. V K$\beta_{5,2}$ emission spectra for mesoporous V–TiO$_2$ as (a) untreated in argon, (b) in 0.37 kPa of water, and (c–f) in 4.3 kPa (constant) of ethanol under visible light (>420 nm) for 1.2 (c), 3.3 (d), 11.9 (e), and 22.4 h (f). The excitation energy was set to 5483.6 eV. Spectrum deconvolutions are depicted as dotted lines (each peak component and the sum) with Lorentz functions for spectra a and f. The longer/black and shorter/red arrows indicate peak top and tune energy (denoted as "TE") for the measurements in Figure 4, respectively.

peak energy before visible light illumination (5461.6 eV[19]), the peak energy shifted by 0.6 eV toward lower energy for 1.2–11.9 h (spectra c–e) and then further by 0.8 eV toward lower energy for 22.4 h (spectrum-f; Table 2A). The shoulder on the lower energy side was not as well resolved for mesoporous V–TiO$_2$ as for fresh catalyst (spectrum-a) or in the presence of 0.37 kPa of water (spectrum-b). The shoulder peak (5457.8–5458.2 eV) was resolved from the major peak and the peak intensity progressively grew over 1.2–22.4 h (spectra c–f).

The K$\beta_{5,2}$ emission spectra a and f were deconvoluted with a minimum number of Lorentz functions. The spectrum-a for fresh sample was fitted with two Lorentz functions (Figure 3a, dotted lines) centered at 5462.1 (main) and 5458.6 eV (side) (Table 2B). Spectrum-f required four Lorentz functions for fitting (Figure 3f, dotted lines). The four components may be considered to be main peaks at 5461.2 and 5459.5 eV accompanied with side peaks at 5457.4 and 5455.7 eV, respectively (Table 2B).

V K$\beta_{5,2}$-Selecting V K-Edge XANES Tuned to V K$\beta_{5,2}$ Main Peak. V K$\beta_{5,2}$-selecting XANES (X-ray absorption near-edge structure) spectra were measured for the mesoporous V–TiO$_2$. The tune energy was first fixed to the main peaks (short/red arrows in Figure 3). First, the V K$\beta_{5,2}$-selecting XANES spectrum for fresh sample was compared to that measured in transmission mode (Figures 4a and 4b). The enhanced peak feature at 5486 and 5504 eV for spectrum-a was due to a resonance excitation effect reported for Fe K$\beta_{1,3}$-selecting,[25] Cu Kα_1-selecting,[21] Sn Kα_1-selecting,[21] and Pb Lα_1-selecting XANES spectra.[21]

Table 2. (**A**) Energy Values for Vanadium K$\beta_{5,2}$ Emission Peaks, Pre-Edge Peaks, and Vanadium K Absorption Edges and (**B**) Peak Deconvolution Results to Vanadium K$\beta_{5,2}$ Emission for Mesoporous V–TiO$_2$ Catalyst[a]

(A)

Sample, conditions	Energy/eV			
mesoporous V–TiO$_2$	K$\beta_{5,2}$ emission	Pre-edge peak	K absorption	Refs.
Incipient (fresh)	5462.1	5468.8	5479.7	This work
In 0.37 kPa of water	5461.3	5468.5	5479.2	This work
In 4.3 kPa of ethanol under visible light				
0 h	5461.6	5468.0	5479.3	19
1.2 h	5461.0, 5457.8(w)			This work
3.3 h[b]	5461.0, 5458.0(w)	5468.0	5479.0	This work
11.9 h[c]	5461.0, 5458.2(m)	5468.4	5477.7	This work
22.4 h[d]	5460.2, 5457.8(m)	5468.1	5476.9	This work

(B)

	Peak energy/eV; Area/10^{-5} eV[e]			
In 4.3 kPa of ethanol under visible light	Side-2	Side-1	Main-2	Main-1
0 h		5458.6; 1.1		5462.1; 5.0
22.4 h	5455.7; 0.98	5457.4; 1.1	5459.5; 3.2	5461.2; 2.6

	Peak height at 5458.0 eV (tune energy for Figure 4f)/10^{-5}			
In 4.3 kPa of ethanol under visible light	Side-2	Side-1	Main-2	Main-1
22.4 h	0.11	0.33	0.50	0.19

a) 3.0 wt % of V. b) At 7.0 h for X-ray absorption measurements. c) At 17.3 h for X-ray absorption measurements. d) At 27.7 h for X-ray absorption measurements. e) Approximated to (peak height) × (full width at the half maximum).
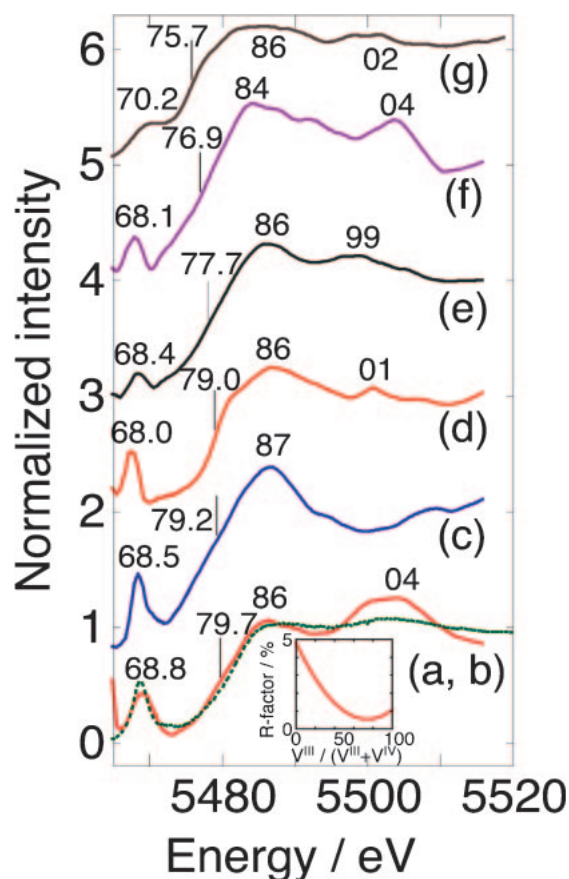
Figure 4. V$K\beta_{5,2}$-selecting V K-edge XANES spectra for mesoporous V–TiO₂ as (a, solid line) untreated, kept under argon, (c) in 0.37 kPa of water, and (d–f) in 4.3 kPa (constant) of ethanol under visible light (>420 nm) for 7.0 (d), 17.3 (e), and 27.7 h (f) and for V₂O₃ diluted with boron nitride (3.0 wt % V; g). The tune energy values were 5462.4, 5461.7, 5460.9, 5460.9, 5458.0, and 5458.7 eV, respectively. Spectrum-b (dotted line) is the corresponding data for spectrum-a, measured in transmission mode.

With the introduction of 0.37 kPa of water, the vanadium K absorption edge shifted by 0.5 eV toward lower energy (Figure 4c), consistent with the negative energy shift of the V$K\beta_{5,2}$ main peak (Figures 3a and 3b and Table 2A). The spectral pattern in which a dominant peak appeared at 5487 eV resembled that for V$K\alpha_1$-selecting XAFS measured for impregnated V/TiO₂ (Degussa P25; anatase:rutile = 7:3) in 0.85 kPa of water at 290 K.[18] The growth of a post-edge peak at 5487 eV was also reported for hydrated V species supported on SiO₂ and Al₂O₃.[26] However, absorption edge energy shifted toward higher energy (+0.4 eV) with water adsorption on V/TiO₂ (crystalline). This difference may be due to the structural difference of V sites. The polymerization suggested to occur for surface V species on V/TiO₂ (crystalline)[18] should not take place for V sites substituting for Ti atoms in the mesoporous TiO₂ matrix used in this work.[18,19]

Next, time course changes of V$K\beta_{5,2}$-selecting XAFS were monitored for fresh mesoporous V–TiO₂ in 4.3 kPa (constant) of ethanol under visible light. The vanadium K absorption edge energy for one ethanol-adsorbed (Table 2A) progressive-

ly shifted by 0.3 eV toward lower energy over 7 h (spectrum-d), and further by 0.3 eV by 17.3 h (spectrum-e). The reaction time is the average for each spectrum measurement because it took several hours to measure one V$K\beta_{5,2}$-selecting XANES spectrum. The pre-edge peak intensity appearing at 5468.0–5468.8 eV gradually became weaker as the photoreaction proceeded (Figures 4a, 4d, and 4e).

V$K\beta_{5,2}$-Selecting V K-Edge XANES Tuned to V$K\beta_{5,2}$ Side Peak. The V K-edge XANES spectrum was measured for mesoporous V–TiO₂ under visible light tuning the spectrometer to 5458.0 eV at the end of photo-catalytic monitoring in ethanol (27.7 h). A lower energy shoulder peak was chosen as tune energy (Figure 3f, short/red arrow) to extract photoreduced V species selectively.

The obtained vanadium K-edge XANES spectrum (Figure 4f) was compared to the weighted sum of spectrum-a measured for fresh mesoporous V^{IV}–TiO₂ and spectrum-g measured for V₂O₃ crystalline (V^{III} sites). The best fit was with a mixing ratio of 25:75 ($R_f = 0.54\%$; Figure 4, inset).

Discussion

Kinetics vis-a-vis X-ray Spectroscopies. Under visible light, in clear contrast to inactive mesoporous TiO₂ (uniformly distributed pores centered at 3 nm[27]), mesoporous V-doped TiO₂ specifically catalyzed oxidative dehydrogenation of ethanol (Figure 1A). A similar doping effect of V^{IV} in sol–gel synthesized TiO₂ has also been reported for the decomposition of crystal violet and methylene blue under visible light.[28] The reaction was found to require molecular oxygen because the ethanol decomposition rate to acetaldehyde in the absence of O₂ on mesoporous V–TiO₂ was only 10% of that in ethanol + O₂ (Table 1, Entries A and B).

Because the energy shifts of the V$K\beta_{5,2}$ emission peak and V K-edge absorption edge were significant (−0.5 and −1.7 eV, respectively) upon ethanol adsorption for incipient mesoporous V–TiO₂,[19] ethoxyl groups should be the major surface species bound to V. The V$K\beta_{5,2}$ emission main peak for catalyst ethanol-adsorbed[17] shifted by −0.6 eV under visible light over 1.2–11.9 h (Figures 3c–3e and Table 2). The emission spectrum in ethanol under visible light for 22.4 h required a minimum of four Lorentz functions for fitting (Figure 3f and Table 2B) compared to two functions for the spectrum of untreated material (Figure 3a). The new main peak at 5459.5 eV was in the energy range of V^{III} species (5458.8–5460.5 eV), separated by 1.7 eV from another main peak assignable to CH₃CH₂O–V$^{IV-\delta}$ species (Figure 5b). The methanol dehydrogenation mechanism was theoretically studied for V/TiO₂ catalyst using density functional theory calculations.[29] Dissociative adsorption of methoxy intermediate followed by H atom subtraction from the substrate to surface V=O species was suggested as the mechanism. In the case of V^{IV} substituted sites in the TiO₂ matrix in this study,[18,19] the presence of V=O double bonds is unlikely. Based on kinetic measurements in ethanol (Figure 1B), the reduced species should be H–V^{III} as a result of H subtraction from ethoxyl followed by desorption of acetaldehyde (Figures 5b and 5c). The two side peaks at 5455.7 and 5457.4 eV are associated with main peaks at 5459.5 and 5461.2 eV, respectively, separated by 3.8 eV from the main peaks.
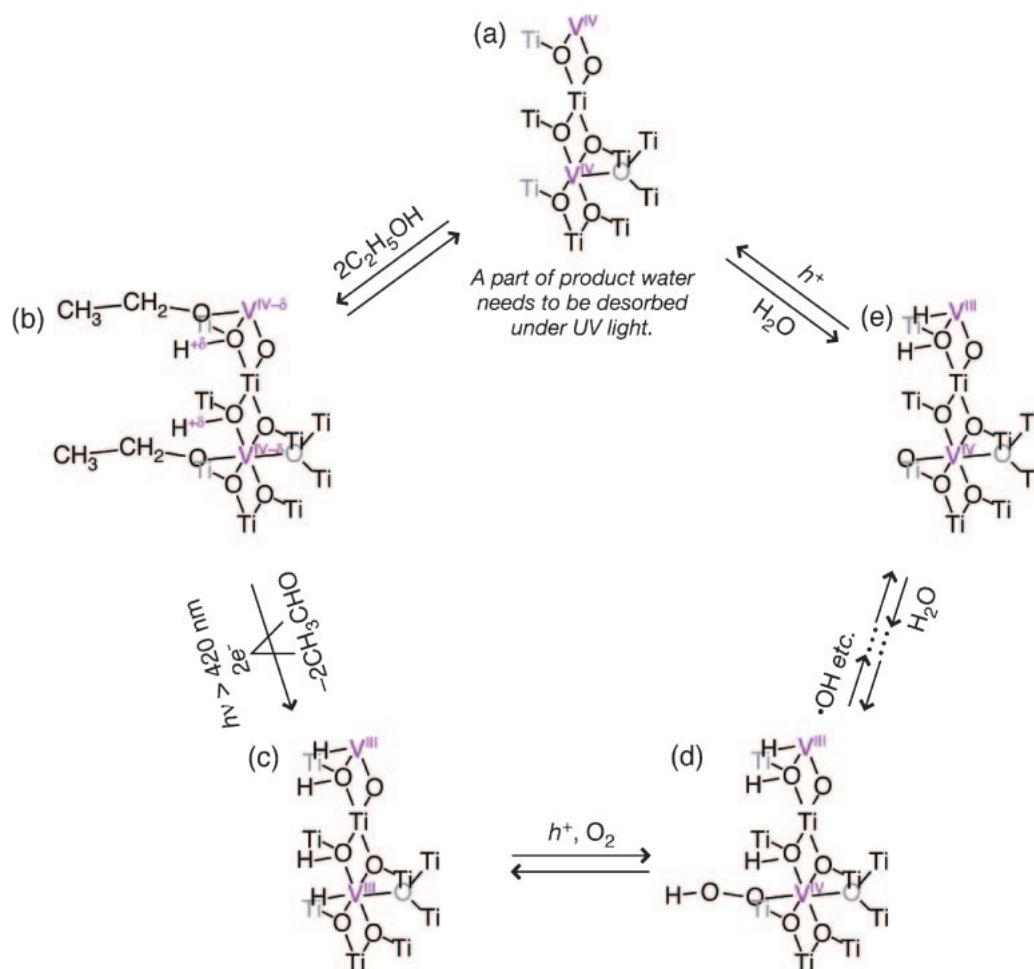
Figure 5. Proposed reaction mechanism of ethanol oxidative dehydrogenation based on several kinetic studies, XRF, and V^{III}/V^{IV}-state selective XAFS.

Based on the main XRF peak area (Table 2B), 55% of V^{IV} sites were reduced to V^{III} (Figure 5c) under visible light over 22.4 h. This ratio corresponds to a reduction rate of 14 μmol-V h^{-1} g$_{catalyst}^{-1}$ from V^{IV} to V^{III}, 5.8 times greater than acetaldehyde formation in ethanol under visible light (Table 1B). One of the possibilities of this discrepancy is re-adsorption of product acetaldehyde on the catalyst surface. Another possibility is that polymerization took place and the product was not detected by GC. However, the reactivity of photo-catalysis was repeated fairly well as shown in Figure 2. Thus, the polymerization should be a minor path if it proceeds. Active V^{IV} species cannot be recreated by oxidation in ethanol gas only. The estimated reduction rate from V^{IV} to V^{III} was comparable to the steady acetaldehyde synthesis rate (23 μmol h^{-1} g$_{catalyst}^{-1}$) in ethanol + O$_2$ measured for 5 h (Table 1A) taking the gradual catalytic deactivation (Figure 1A) for 22.4 h into account. The acetaldehyde desorption step was found to be rate-limiting (Figures 5b and 5c) in the oxidative dehydrogenation of ethanol followed by quicker photo-oxidation steps.

It is evident that the rate-limiting step requires light because the photo-catalytic activity gradually decreased when the UV-cut was progressively changed from 370 to 580 nm (Figure 6). The red-ox potential of methanol reduction to formaldehyde is
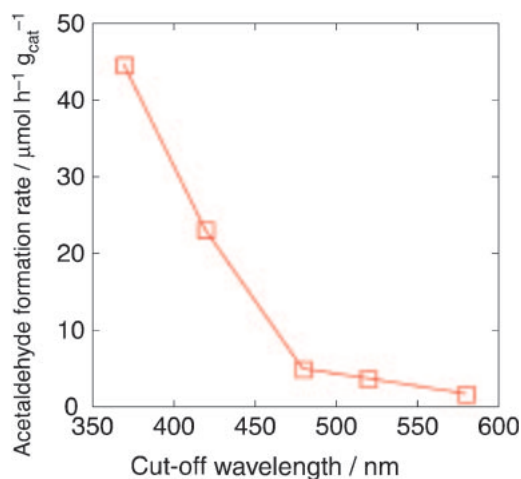
Figure 6. The acetaldehyde formation rate dependence on UV cut-off wavelength. The reaction conditions were same as in Figure 1A. UV-cut filters L37, L42, Y48, Y52, and O58 were used at the exit of the xenon arc lamp.

+0.04 V. The conduction and valence band levels for mesoporous V–TiO$_2$ should be smaller/greater than -0.52 and $+2.53$ V, respectively,[3] for rutile-type TiO$_2$ because of the band gap growth due to quantum size effect.[12] The band gap

for mesoporous V–TiO$_2$ was estimated to be 2.67 eV.[13] Thus, the impurity energy level for V substitution at the matrix Ti sites is −0.14 eV or greater. The red-ox potential for ethanol reduction to acetaldehyde may be greater than the V impurity energy level and the reaction mechanism illustrated in Figure 5 was enabled.

The V sites were also monitored using state-selective V K-edge XAFS under several catalytic conditions (Figure 4). The tune energies between 5462.4 and 5460.9 eV for Figures 4a, 4c, 4d, and 4e were in the energy region for standard inorganic V^{IV} compounds.[19] The main peak at 5462.1 eV accompanied a lower energy side peak, separated by 3.5 eV for untreated mesoporous V–TiO$_2$ (Table 2B). The chemical shift on going from V^{IV} to V^{III} states is also toward lower energy, e.g. −3.2 eV on going from V^{IV}O(SO$_4$)·nH$_2$O to V$^{III}_2$O$_3$.[19] Thus, the tune energies between 5462.4 and 5460.9 eV include smaller contribution from V^{III} sites and the V^{IV} states in the samples were preferably monitored in the V K$\beta_{5,2}$-selecting XAFS measurements (Figures 4a, 4c, 4d, and 4e) compared to conventional XAFS data (Figure 4b).

The V K absorption edge shifted toward lower energy in ethanol under visible light over 0–17.3 h (−0.4− −2.0 eV, Table 2A) within the energy range for V^{IV} (5476.9–5479.8 eV). Progressive photo-reduction from V^{IV} to V^{III} was suggested (Figure 5c). V^{III} sites should co-exist in samples for spectra d and e, but due to V^{IV}-selective measurements tuned to 5460.9 eV, the rising edge positions were in the energy range for V^{IV}. Decrease of pre-edge peak intensity appeared at 5468.0–5468.8 eV on going from Figure 4a (untreated) to d (7.0 h) and then to e (17.3 h) suggesting an increase of V site symmetry due to the coordination of intermediate species (Figures 5b and 5c).

The selection of V^{III} was tried in V K$\beta_{5,2}$-selecting XANES tuned to 5458.0 eV in ethanol under visible light for 27.7 h (Figure 4f). Deconvoluted side peak-1 was at 5457.4 eV (Table 2B) near the tune energy. Based on the V K$\beta_{5,2}$ emission peak intensity of main peak-1 (V^{IV}) and main peak-2 (V^{III}), the population of V^{III} sites was evaluated to be 55% under those conditions. If we assume that the side peaks at 5457.4 and 5455.7 eV were accompanied by main peaks-1 and -2, respectively, the sum of contributions of main peak-2 and side peak-2 (V^{III} state) was 54% at 5458.0 eV (Table 2B). Thus, unfortunately site selection was not effective in the XANES measurement tuned to 5458.0 eV.

The selection of V^{III} in the XANES spectrum-f (Figure 4) was evaluated to 75% (Figure 4, inset) based on comparison to the weighted sum of V K$\beta_{5,2}$-selecting XANES data for untreated V^{IV} (Figure 4a) and reference V^{III} state (g). The higher V^{III} site ratio in XANES (75%) compared to 55% in XRF may be a result of the difference in photo-reaction time (27.7 and 22.4 h, respectively). Thus, the V^{III} site structure in the catalyst was similar to that in V$_2$O$_3$ except for the difference of coordination number of V–O (4–5 vs. 6, respectively).

The oxidative dehydrogenation also proceeded for ethanol pre-adsorbed mesoporous V–TiO$_2$ (Figure 1C). This is the reaction of dissociatively adsorbed ethoxyl (Figure 5b) with gaseous O$_2$. The formation rates of acetaldehyde and water were both 38% of the corresponding rates in ethanol + O$_2$ (Table 1, Entries A and C). The consumption/formation rate depen-

dence on O$_2$ gas pressure was less than one order, probably a half order. The reverse reaction rate to form ethanol was 220% of the acetaldehyde formation rate in ethanol + O$_2$. A step of H subtraction from ethoxyl species (Figures 5b and 5c) and subsequent O$_2$ adsorption (d) were suggested for this kinetic measurement. In the steps from states d to e, reactive •OH radical species may be also formed with holes.[17,30,31]

A proposed reaction cycle of ethanol oxidative dehydrogenation is illustrated in Figure 5. For mesoporous V–TiO$_2$ in ethanol gas only (Figure 1B for kinetics, Figures 3a and 3c–3f for XRF, and Figures 4a and 4d–4f for XANES), transformation from Figure 5a to 5b and then 5c was monitored. In the oxidation of ethanol pre-adsorbed catalyst (Figure 1C), transformation from Figure 5b to 5c, 5d, 5e, and then finally to 5a should take place, but the reverse reaction from Figure 5b to 5a was also observed in the absence of gas-phase ethanol. Because the formation of water is typical for mesoporous V–TiO$_2$ and it is not formed on crystalline TiO$_2$ either doped or not doped with vanadium,[13] the structures d and e should be specific for mesoporous V–TiO$_2$ for selective activation of O$_2$.

Amorphous TiO$_2$ and/or V^{IV} sites substitution for the Ti atoms generally leads to electron–hole recombination.[2,17,30] Improved oxidative dehydrogenation activity found for mesoporous V–TiO$_2$ (Table 1, Entry A) may be due to unsaturated coordination of V and extremely high specific SA (1000 m^2 g^{-1}).

Poisoning with Water and Re-activation in UV Light. In the ethanol oxidation over mesoporous V–TiO$_2$, quicker water formation was observed in the first 1 h, and then water and acetaldehyde formation reached a steady state (Figure 1A). After the catalyst was in 1.73 kPa of water, water was not produced in ethanol + O$_2$ under visible light (Figure 1B) and the formation rate of acetaldehyde was 52% of that over untreated mesoporous V–TiO$_2$ (Table 1, Entries A and D).

Partial reduction of V^{IV} sites was suggested based on the peak shifts toward lower energy in the V K$\beta_{5,2}$ emission spectra (−0.8 eV, Figures 3a and 3b) and V K-edge absorption edge (−0.5 eV, Figure 4c) in moisture. The V K$\beta_{5,2}$ peak energy (5461.3 eV), V K absorption edge energy (5479.2 eV), post-edge intense peak energy (5487 eV), and XANES profile in the range of 5465–5515 eV (Figures 3b and 4c) were most similar to those for the catalyst in 2.1 kPa of ethanol.[19] Therefore, dissociatively adsorbed water blocked active V^{IV} sites and induced partial negative charge donation to the V^{IV} sites. The surface agglomeration of VO$_x$ species on crystalline TiO$_2$[18] did not take place.

Based on kinetic and X-ray spectroscopic implication, mesoporous V–TiO$_2$ was treated under UV–visible light between catalytic reaction batches (Figure 2). The initial formation rates of acetaldehyde and water in the second and third batches were 108–52% of the corresponding rates in the first batch. Time course profiles of initial water formation and steady state formation for both products were repeated. Thus, a major portion of water molecules blocking the V sites was desorbed under UV light. The water desorption under UV light can be understood from the energy diagram.[3] The red-ox potential between dissociatively adsorbed two hydroxyl species and water may be similar to that for H$_2$/H$_2$O (−0.41 V).

The valence band level for mesoporous V–TiO$_2$ should be greater than +2.53 V[3] for rutile-type TiO$_2$ due to quantum size effects.[12] Thus, UV light shorter than 420 nm was required for water desorption.

Conclusion

The kinetic measurements and on-reaction X-ray spectroscopic monitoring for specific oxidative dehydrogenation of ethanol over mesoporous V/TiO$_2$ under visible light were correlated. Because the transformation rate from V^{IV} to V^{III} in the catalyst monitored by V K$\beta_{5,2}$ emission spectra was comparable to the catalytic acetaldehyde synthesis rate in ethanol + O$_2$, the desorption step of acetaldehyde formed by H subtraction from ethoxyl species bound to surface V sites was found to be rate-limiting.

The synthesis rates of acetaldehyde and water in O$_2$ for ethanol pre-adsorbed mesoporous V–TiO$_2$ were both 38% of the corresponding rates in ethanol + O$_2$, but the reverse reaction rate to form ethanol was 220% of the acetaldehyde formation rate in ethanol + O$_2$. The consumption/synthesis rate dependence on O$_2$ pressure was less than one. The oxidation steps of H–V^{III} seem to be more quickly activated as HOO–V^{IV} and/or •OH species under visible light.

Dissociative adsorption of water on V sites was confirmed based on the V K$\beta_{5,2}$ emission and V K$\beta_{5,2}$-selecting XANES. Water pre-adsorbed mesoporous V–TiO$_2$ catalyst produced only acetaldehyde at a rate 52% of that over untreated catalyst. To overcome the problem of water poisoning, reactivation was attempted by illuminating the catalyst under UV light between catalytic batches. The formation rates of acetaldehyde and water in the second and third batches were 108–52% of corresponding rates in the first batch. The inconsistency of the formed amounts of acetaldehyde and water may be due to re-adsorption and/or polymerization of acetaldehyde. Re-adsorbed acetaldehyde or polymerized species should be desorbed during UV light illumination.

References

1 Part 28 of state-selective X-ray absorption fine structure series.

2 M. R. Hoffmann, S. T. Martin, W. Choi, D. W. Bahnemann, *Chem. Rev.* **1995**, *95*, 69.

3 A. Fujishima, T. N. Rao, D. A. Tryk, *J. Photochem. Photobiol., C* **2000**, *1*, 1.

4 X. Chen, S. S. Mao, *Chem. Rev.* **2007**, *107*, 2891.

5 S. K. Mohapatra, M. Misra, V. K. Mahajan, K. S. Raja, *J. Phys. Chem. C* **2007**, *111*, 8677.

6 R. Asahi, T. Morikawa, T. Ohwaki, K. Aoki, Y. Taga, *Science* **2001**, *293*, 269.

7 A. R. Gandhe, S. P. Naik, J. B. Fernandes, *Microporous Mesoporous Mater.* **2005**, *87*, 103.

8 Y. Cong, J. Zhang, F. Chen, M. Anpo, *J. Phys. Chem. C* **2007**, *111*, 6976.

9 J. G. Yu, J. C. Yu, B. Cheng, S. K. Hark, K. Iu, *J. Solid State Chem.* **2003**, *174*, 372.

10 D. Zhao, C. Chen, Y. Wang, W. Ma, J. Zhao, T. Rajh, L. Zang, *Environ. Sci. Technol.* **2008**, *42*, 308.

11 Y. Murakami, B. Kasahara, Y. Nosaka, *Chem. Lett.* **2007**, *36*, 330.

12 M. Anpo, *Bull. Chem. Soc. Jpn.* **2004**, *77*, 1427.

13 D. Masih, H. Yoshitake, Y. Izumi, *Appl. Catal., A* **2007**, *325*, 276.

14 M. S. Nahar, K. Hasegawa, S. Kagaya, S. Kuroda, *Bull. Chem. Soc. Jpn.* **2007**, *80*, 1017.

15 G. Liu, Z. Chen, C. Dong, Y. Zhao, F. Li, G. Q. Lu, H. M. Cheng, *J. Phys. Chem. B* **2006**, *110*, 20823.

16 S. Usseglio, A. Damin, D. Scarano, S. Bordiga, A. Zecchina, C. Lamberti, *J. Am. Chem. Soc.* **2007**, *129*, 2822.

17 Y. Shiraishi, N. Saito, T. Hirai, *J. Am. Chem. Soc.* **2005**, *127*, 12820.

18 Y. Izumi, F. Kiyotaki, N. Yagi, A. M. Vlaicu, A. Nisawa, S. Fukushima, H. Yoshitake, Y. Iwasawa, *J. Phys. Chem. B* **2005**, *109*, 14884.

19 Y. Izumi, K. Konishi, D. M. Obaid, T. Miyajima, H. Yoshitake, *Anal. Chem.* **2007**, *79*, 6933.

20 H. Yoshitake, T. Tatsumi, *Chem. Mater.* **2003**, *15*, 1695.

21 Y. Izumi, H. Nagamori, F. Kiyotaki, D. Masih, T. Minato, E. Roisin, J. P. Candy, H. Tanida, T. Uruga, *Anal. Chem.* **2005**, *77*, 6969.

22 Y. Izumi, F. Kiyotaki, H. Nagamori, T. Minato, *J. Electron. Spectrosc. Relat. Phenom.* **2001**, *119*, 193.

23 J. A. Bearden, *Rev. Mod. Phys.* **1967**, *39*, 78.

24 G. Zschornack, *Handbook of X-ray Data*, Springer, Berlin/Heidelberg, **2007**.

25 W. M. Heijboer, P. Glatzel, K. R. Sawant, R. F. Lobo, U. Bergmann, R. A. Barrea, D. C. Koningsberger, B. M. Weckhuysen, F. M. F. de Groot, *J. Phys. Chem. B* **2004**, *108*, 8876.

26 B. Olthof, A. Khodakov, A. T. Bell, E. Iglesia, *J. Phys. Chem. B* **2000**, *104*, 1516.

27 H. Yoshitake, T. Sugihara, T. Tatsumi, *Chem. Mater.* **2002**, *14*, 1023.

28 J. C. S. Wu, C. H. Chen, *J. Photochem. Photobiol., A* **2004**, *163*, 509.

29 R. Z. Khaliullin, A. T. Bell, *J. Phys. Chem. B* **2002**, *106*, 7832.

30 S. T. Martin, C. L. Morrison, M. R. Hoffmann, *J. Phys. Chem.* **1994**, *98*, 13695.

31 A. Lu, Y. Li, M. Lv, C. Wang, L. Yang, J. Liu, Y. Wang, K. H. Wong, P. K. Wong, *Sol. Energy Mater. Sol. Cells* **2007**, *91*, 1849.